Autophagy

Volume 11 - Issue 11 - November 2015

Editor-in-Chief
Daniel J. Klionsky
University of Michigan

Taylor & Francis
Taylor & Francis Group

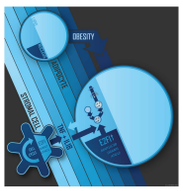


Autophagy

ISSN: (Print) (Online) Journal homepage: https://www.tandfonline.com/loi/kaup20

# Regulation of autophagy by DNA G-quadruplexes

Pauline Lejault , Jose F. Moruno-Manchon , Sree M. Vemu , Pedram Honarpisheh , Liang Zhu , Nayun Kim , Akihiko Urayama , David Monchaud , Louise D. McCullough & Andrey S. Tsvetkov

**To cite this article:** Pauline Lejault , Jose F. Moruno-Manchon , Sree M. Vemu , Pedram Honarpisheh , Liang Zhu , Nayun Kim , Akihiko Urayama , David Monchaud , Louise D. McCullough & Andrey S. Tsvetkov (2020): Regulation of autophagy by DNA G-quadruplexes, Autophagy, DOI: 10.1080/15548627.2020.1769991

**To link to this article:** https://doi.org/10.1080/15548627.2020.1769991

Accepted author version posted online: 18 May 2020.

**Publisher:** Taylor & Francis & Informa UK Limited, trading as Taylor & Francis Group

**Journal:** *Autophagy*

**DOI:** 10.1080/15548627.2020.1769991

Manuscript Section: **Addendum**

# Regulation of autophagy by DNA G-quadruplexes

Pauline Lejault[1§], Jose F. Moruno-Manchon[2§], Sree M. Vemu[3], Pedram Honarpisheh[2,7], Liang Zhu[4,5], Nayun Kim[6,7], Akihiko Urayama[2,7], David Monchaud[1], Louise D. McCullough[2,7] and Andrey S. Tsvetkov[2,7,8*]

[1]Institut de Chimie Moléculaire (ICMUB), UBFC Dijon, CNRS UMR6302, 9, Rue Alain Savary, 21078, Dijon, France
[2]Department of Neurology, the University of Texas McGovern Medical School at Houston, TX
[3]Summer Research Program, The University of Texas Medical School at Houston, TX
[4]Biostatistics and Epidemiology Research Design Core Center for Clinical and Translational Sciences, The University of Texas McGovern Medical School at Houston, Houston, TX
[5]Department of Internal Medicine, The University of Texas McGovern Medical School at Houston, Houston, United States;
[6]Department of Microbiology and Molecular Genetics, the University of Texas McGovern Medical School at Houston, TX
[7]The University of Texas Graduate School of Biomedical Sciences, Houston, TX
[8]UTHealth Consortium on Aging, the University of Texas McGovern Medical School, Houston, TX

§ Authors contributed equally to this work

*Correspondence to: Andrey S. Tsvetkov, PhD, Department of Neurobiology and Anatomy, University of Texas Medical School, 6431 Fannin St., MSB 7.258, Houston, TX 77030

E-mail: Andrey.S.Tsvetkov@uth.tmc.edu

No. of figures: 3

Key words: aging; astrocytes; autophagy; G-quadruplex; neurodegeneration; neurons

We have no conflict of interest to declare.

**Abstract**

Guanine-rich DNA strands can form secondary structures known as G-quadruplexes (G4-DNA). G4-DNA is important for the regulation of replication and transcription. We recently showed that the expression of *Atg7*, a gene that is critical for macroautophagy/autophagy, is controlled by G4-DNA in neurons. We demonstrated that the transcription factor SUB1/PC4 and the G4-DNA-specific antibody HF2 bind to a putative G4-DNA motif located in the *Atg7* gene. Stabilizing G4-DNA with the G4-ligand pyridostatin (PDS) downregulates *Atg7* expression in neurons. Here, we further investigated how G4-DNA in the *Atg7* gene is stabilized by PDS. We show that PDS can form 1:1 and 2:1 complexes with the *Atg7*'s G4. We also demonstrate that PDS downregulates the ATG7 protein and the expression of *Atg7* in astrocytes as well as in neurons. Together with our previous findings, these data establish a novel G4-DNA-associated mechanism of autophagy regulation at a transcriptional level in neurons and astrocytes.

**Manuscript**

G-quadruplex DNA (G4-DNA or G4) is a secondary DNA structure formed within guanine (G)-rich strands *via* self-association of four guanines to form G-quartets. Stacking and stabilization of these G-quartets are promoted by the coordination of certain cations (*e.g.*, by potassium). G4-DNA regulates DNA replication, recombination, transcription, and telomere maintenance [1, 2]. Putative G4-DNA motifs occur approximately once per 10 kb in the human genome and are frequently present in promoters, oncogenes, and regulatory genes regions [3-5]. G4-DNA-binding proteins and G4-DNA unwinding helicases associate with and regulate G4-DNA [6-10]. Evidence indicates that these proteins regulate transcription of genes that contain G4-DNA [11, 12]. In yeast, Sub1, a homolog of the mammalian transcription factor SUB1/PC4, interacts with the G4 helicase Pif1 to suppress G4-induced genomic instability by facilitating G4-DNA unfolding and enhancing transcription [13].

G4-DNA is also implicated in neurological diseases. An expansion of a non-coding GGGGCC repeat in the gene *C9orf72* is associated with 10% of familial cases of frontotemporal

dementia and amyotrophic lateral sclerosis [14]. The repeats form DNA, RNA, and DNA-RNA G4s, leading to an accumulation of ribonucleoprotein complexes that hamper nucleocytoplasmic trafficking and increase intranuclear stress [15, 16]. G4-DNA is also implicated in Fragile X syndrome, which is caused by trinucleotide CGG repeat expansion. These abnormally expanded CGG repeats fold into a G4 structure and silence the *FMR1*/fragile X mental retardation 1 gene [17]. Moreover, mutations in genes encoding DNA helicases are linked to other G4-DNA-related disorders, such as Werner syndrome with premature aging, Bloom syndrome with skin rash, developmental abnormalities, and predisposition to cancer, and Cockayne syndrome characterized by neurodegeneration and premature aging [18, 19].

We recently demonstrated that G4-DNA plays a role in neuronal macroautophagy/autophagy. Autophagy is a fundamental intracellular process that removes aggregated proteins, senescent organelles, and parasites [20]. Autophagy is critical for cell survival and maintenance, proteostasis, organelle quality control, and prevention of cellular senescence and aging, among other processes [20]. The autophagic pathway is orchestrated by the autophagy-related (ATG) proteins, which nucleate the autophagosomal precursor phagophore and elongate the autophagosome, engulf a cytoplasmic cargo, and fuse the autophagosome with the lysosome [20]. Autophagy is regulated by transcription and translation, as well as by protein post-translational modifications [21]. A number of studies demonstrated that autophagic genes are subject to epigenetic silencing [22, 23]. Autophagy plays a positive role in longevity and deceleration of the aging process [24]. Recent studies have shown that autophagy-related genes are critical for longer healthspan and lifespan in worms, flies, and mice [24, 25]. The expression of important autophagic genes such as *Becn1* (beclin 1), *Atg5* and *Atg7,* which are epigenetically regulated [26], diminishes with aging [27].

ATG7 is an E1-like enzyme that couples LC3-I to the E2-like enzyme ATG3 and leads to the E3-like complex ATG12–ATG5-ATG16L1. This E3-like complex then conjugates LC3-I to phosphatidylethanolamine in phagophore membranes, which is a critical step in autophagosome biogenesis [20]. Strong evidence supports the role of *Atg7* in neurodegeneration. *Atg7/ATG7* is found to be downregulated in pre-clinical models of alpha-synucleinopathy and brain samples from patients with Lewy Body disease, suggesting a possible contribution of defective autophagy in the pathogenesis of this disorder. Increasing *Atg7 via* lentiviral delivery decreases the levels of SNCA (synuclein alpha) and mitigates neurodegeneration [28]. Deletion of *Atg7* in Purkinje cells

results in neurodegeneration [29]. Degeneration of *Atg7*-deficient neurons in the midbrain of conditional *atg7* knockout mice is accompanied by the formation of ubiquitinated inclusion bodies [30]. The expression of *ATG7* is reduced in the human brain during normal aging [27]. *ATG7* and its homologs are regulated by histone and chromatin modifications in flies, worms, and human non-neuronal cells [31, 32].

The *ATG7/Atg7* gene (human, mouse, rat) contains numerous putative G4-forming motifs[33]. We recently investigated whether pharmacologically stabilizing G4-DNA with pyridostatin (PDS) [34], a selective G4-binding small molecule (referred to as a G4-ligand [35]), affects neuronal autophagy. Using circular dichroism spectroscopy (CD), thermal difference spectra (TDS) and nuclear magnetic resonance (NMR) analyses, we demonstrated that a putative G4-DNA forming sequence (PQFS) identified in the *Atg7* gene folds into a stable G4 structure *in vitro*, which PDS strongly binds to [33]. We next showed that the G4-specific antibody (HF2) and the G4-binding protein SUB1/PC4 bind to the *Atg7*'s PQFS (**Fig. 1A**; a scheme of the *Atg7* gene) [33]. Cultured cortical neurons treated with PDS exhibited diminished *Atg7* expression and reduced autophagy [33]. Mice treated with PDS exhibited memory deficits and accumulation of lipofuscin [33]. We also discovered that G4-DNA is abundantly present in aged mouse brain, but not in the brains of young mice [33].

Our findings indicate that an age-associated change in DNA conformation *via* the formation of stable G4-DNA could be a novel mechanism of autophagy regulation in aging neurons. Our data also suggest that anti-neoplastic agents that target G4-DNA [36] (*i.e.*, G4-ligands) may accelerate brain aging and lead to neurodegenerative diseases.

Importantly, our previous findings indicate that endogenous G4-DNA ligands, small molecules or proteins, may regulate neuronal transcription in general and the expression of *Atg7* in particular, thereby modulating autophagy. To go a step further, we investigated a mechanism of PDS interaction with a G4-DNA motif from the *Atg7* gene, so called *Atg7-32*, that we discovered previously (**Fig. 1A**). The *Atg7-32* motif (d[$^{5'}G_4CTG_4TC_3T_2G_4A_2CTGTAT_2G_3{}^{3'}$]), a 32-nt G-rich sequence, was demonstrated to adopt a stable G4-DNA structure *in vitro* by CD, TDS and NMR. Here, we used the electrospray ionization mass spectrometry (ESI-MS) technique as it allows measuring both the stoichiometry and equilibrium binding constant of the non-covalent G4-DNA/PDS complexes [37]. With ESI-MS, we showed that a 1:1 mixture of PDS:DNA results in the 1:1 PDS:G4 complex (54.6%), along with unbound DNA (36.4%) and a

fraction of the 2:1 PDS:G4 complex (9%) (**Fig. 1B and 1C**). Increasing amount of PDS to a 2:1 mixture of ligand:DNA results in the 2:1 PDS:G4 complex (60.8%), the 1:1 PDS:G4 complex (38.5%), and some residual unbound DNA (0.7%) (**Fig. 1D**). Our data indicate that PDS has a high affinity for the *Atg7-32* G4 ($K = 1.47x10^7\ M^{-1}$), and that both external G-quartets provide equivalent binding sites for PDS. We then performed a series of control experiments with mutated *Atg7-32* (mut*Atg7-32*; d[$^{5'}$GCGCCTGCGCTC$_3$T$_2$GCGCA$_2$CTGTAT$_2$GCG$^{3'}$]), a DNA sequence that cannot fold into a G4 structure due to the G-to-C mutations (underlined) in *Atg7-32*. We discovered a low affinity, electrostatically driven association of PDS and mut*Atg7-32* ($K = 7.73x10^4\ M^{-1}$) as a 2:1 mixture PDS:mutAtg7-32, which is ~2 orders of a magnitude lower than of *Atg7-32* (**Fig. 1E-G**). We, therefore, confirmed the interaction specificity between PDS and a G4-DNA motif from the *Atg7* gene.

Since neurons are highly specialized post-mitotic cells, we speculated that neuronal G4 pathways may be drastically different from G4-based mechanisms in their dividing symbiotic cells, namely in astrocytes. We first confirmed that our astrocytic cultures [38] are pure astrocytes. Astrocytes were grown in culture in DMEM + serum for 3 weeks, fixed, and stained with fluorescent phalloidin and antibodies against GFAP (**Fig. 2A**). Expectedly, neurons, microglia, and oligodendrocytes, which all require specific medium condition, died off and remaining cells were homogeneous cultures of astrocytes (**Fig. 2A**). We then tested whether stabilizing G4s downregulates *Atg7* in astrocytes, as in neurons, using qRT-PCR. We found that *Atg7*'s mRNA levels were 2-fold lower in PDS-treated compared to vehicle-treated astrocytes (p=0.017) (**Fig. 2B**). *Tbp* (TATA-binding protein) mRNA was used as loading control as neither *Tbp* nor its promoter contains a PQFS [39]. Intriguingly, we had previously shown that expression of *Atg7* was 7-fold lower in PDS-treated compared to vehicle-treated neurons, suggesting that neurons are more sensitive to PDS treatment than astrocytes. Since the levels of *Atg7*'s mRNA are reduced by PDS treatment, we tested if the ATG7 protein is affected by PDS. We found that ATG7 was about 30% lower in astrocytes exposed to PDS than in vehicle-treated astrocytes (p=0.019) (**Fig. 2C and 2D**). As astrocytes basally have low levels of autophagy [38, 40], G4 stabilization still leads to downregulating ATG7 levels in these cells. We also looked at the levels of SQSTM1, which is commonly used as an autophagic reporter. PDS promoted accumulation of SQSTM1 by 2-fold, confirming slowed autophagy (p=0.018) (**Fig. 2C and 2D**).

Next, we confirmed that the flux through autophagy is reduced by PDS with an optical pulse-chase method. The Dendra2-LC3 reporter has been used to study autophagic flux in astrocytes. Astrocytic cultures were transfected with Dendra2-LC3 and photoswitched 24 h thereafter. Co-transfection with the *Sphk1* (sphingosine kinase 1) gene, a genetic enhancer of autophagy [38, 41, 42], was used as a positive control. The decay of "red" Dendra2 was analyzed, and the flux *via* autophagy was measured. PDS inhibited the flux through autophagy (**Fig. 2E and 2F**).

Next, cultured primary astrocytes were treated with either a vehicle or PDS then stained with a G4-DNA fluorophore, N-TASQ that has been used to investigate G4-DNA landscapes in cancer cells [43-45] and neurons [35]. Astrocytes were treated, fixed, permeabilized, and then stained with both N-TASQ (G4s) and DAPI (nuclear DNA). The nuclear puncta index, which is a standard deviation of the intensities measured among pixels within the region of interest (here, the nucleus), was measured. A low index indicates a diffuse N-TASQ nuclear staining while a high index indicates the presence of N-TASQ nuclear *foci*. We found that PDS significantly promotes G4-DNA formation in the astrocytic nuclei ($p<0.0001$) (**Fig. 3A-C**). Intriguingly, we also found that, unlike neuronal cells, both vehicle- and PDS-treated astrocytes contain N-TASQ foci in the cytoplasm. Previously, it was demonstrated that cancerous cells frequently contain N-TASQ foci in the cytoplasm [43-46] (G4-RNA [47]), as cultured astrocytes in our samples. These N-TASQ foci mostly consisted of ribosomal RNA and long non-coding RNA in cancer cells [46]. RNase treatment was thus performed to enhance the contrast of the nuclear staining. We discovered that, in RNase-treated cells, PDS-treated astrocytes exhibit higher levels of N-TASQ fluorescence than vehicle-treated cells, indicating that PDS modulates a G4 landscape in astrocytes, as in neurons (**Fig. 3A-C**). Together, our data indicate that stabilizing G4-DNA with PDS downregulates autophagy in neurons and in astrocytes, suggesting a common mechanism in these symbiotic brain cells.

During aging and age-associated diseases, astrocytic chromatin undergoes epigenetic modifications, including DNA methylation and histone modifications [48]. Our findings demonstrate that stabilized G4-DNA might represent an additional epigenetic-like mechanism that regulates gene expression in astrocytes. Investigating G4-DNA-associated mechanisms in astrocytes and in other cell types in the central nervous system may lead to novel therapies for neurodegenerative disorders.

## Materials and Methods

### *Chemicals, plasmids, and antibodies.*

N-TASQ was synthesized as described [43]. PDS was from Sigma (SML0678) and from Selleck Chemicals (S7444). The DAPI dye was from Thermo Fisher Scientific (D1306). Ribonuclease A (RNase) from bovine pancreas was from Sigma (R4642). pGW1-Dendra2-LC3 and pGW1-SK1 were cloned by us and were described previously [49]. pGW1 (British Biotech, discontinued) was described previously [49]. Antibodies against ACTB/β-actin were from Cell Signaling Technology (clone 8H10D10; 3700; 1:2000). Antibodies against LC3 were from MBL (PD014; 1:1000). Antibodies against SQSTM1/p62 were from BD Biosciences (610833; 1:2000). Antibodies against GFAP were from Santa Cruz Biotechnology (sc-9065; 1:100). Alexa Fluor 633 phalloidin was a gift from Dr. Taeyeop Park (Carmen Dessauer's lab, Integrative Biology and Pharmacology, University of Texas McGovern Medical School) (Thermo Fisher Scientific, A22284). Antibodies against rabbit IgG(H + L) conjugated with horseradish peroxidase (HRP; AP307P; 1:3000), and mouse IgG(H + L) conjugated with horseradish peroxidase (AP308P; 1:3000) were from EMD Millipore.

### *G4-DNA Analyses.*

The QGRS mapper (http://bioinformatics.ramapo.edu/QGRS/index.php) was used to determine the potential G4-DNA structures contained in genes of interest and their G-scores. Search parameters: maximal length: 45; minimal G-group size: 3; loop size: from 0 to 10 [2].

### *Electrospray Ionization Mass Spectrometry.*

Electrospray mass spectrometry experiments were performed on an LTQ Orbitrap XL (Thermo Fisher Scientific) spectrometer equipped with Ion Max source and HESI-II probe in the negative ion mode. Both *Atg7-32* (10 μM) and mut*Atg7-32* (10 μM) alone, as well as the corresponding DNA:PDS mixtures (1:1 and 1:2 mol. equiv.), were prepared in 100 mM ammonium acetate buffer (Sigma, 73594-25G-F) and equilibrated at 25°C for 1 h. To obtain a stable electrospray

signal, 20% of methanol were added to the solution just before injection. The solutions were injected with syringe pump at a flow rate of 5 µL/min. The full scan mass was recorded in 600-4000 m/z range. The following tuning parameters were used: heater temperature = 50°C, spray voltage = 4.0 kV, capillary temperature = 275°C, tube lens = -160.00 (negative ion mode) and the capillary voltage varied between -35.00 V and -60.00 V. Quantification of the equilibrium affinity constants (K) of PDS for Atg7-32 and mutAtg7-32 was done according to Rosu *et al*., *via* the equation $K$ = [DNA:PDS]/([$DNA_{free}$][$PDS_{free}$]) [50].

***Astrocytic Cultures and Treatments.***

Cortices from rat embryos (E17–18) were dissected, dissociated, and plated on 24-well tissue-culture plates ($4x10^5$/well) coated with poly-D-lysine (BD Biosciences, A-003-E). Primary cortical astrocytes were grown in Dulbecco´s Modified Eagle Medium (HyClone, SH3024301) supplemented with 10% heat-inactivated fetal bovine serum (Sigma, F4135) and penicillin-streptomycin as described at least for 3 weeks before experiments [38]. Some cultures were treated with vehicle or PDS (2 µM, overnight). Some astrocytic cultures were fixed with 4% PFA, permeabilized with 0.1% Triton X-100 (Santa Cruz Biotechnology, sc-29112) in PBS (Bio-Rad Laboratories, 161-0780), washed 3 times with PBS, incubated with 1 mg/ml RNase for 1 h at 37°C. Samples were then washed 3 times with PBS and then labeled with N-TASQ (50 µM, overnight, room temperature). Some cultures were transfected with Lipofectamine 2000 (Thermo Fisher Scientific, 11668027) and a total of 1–2 µg of plasmid DNA per well, as described [38].

***Western blotting.***

Western blotting was performed as described [38]. Cleared cellular lysates were analyzed by SDS/PAGE and proteins were transferred onto PVDF membranes (Thermo Fisher Scientific, IB401031) by the iBlot2 system (Thermo Fisher Scientific). Membranes were blocked and incubated overnight with antibodies against ACTB, LC3 or SQSTM1. Membranes were washed and probed for 1 h with anti-rabbit or anti-mouse antibodies conjugated with horseradish

peroxidase. Signals were detected using ProSignal Pico (Genesee Scientific, 20-300B) on Medical X-Ray Film (Kodak, 7400).

***RNA Extraction and qRT-PCR.***

Total RNA was extracted from primary culture using the RNeasy Mini kit (Qiagen, 74104), and then reverse transcribed using iScript Reverse Transcription SuperMix (Bio-Rad, 1708840), according to the manufacturer's protocol and as described [39]. RT-qPCR was performed using a Bio-Rad CFX96 Touch machine using SSoAdvanced Universal SYBR Green (Bio-Rad, 1725275) for visualization and quantification according to the manufacturer's instructions. Primer sequences were: *Atg7*, forward: 5′-$TC_2TGAGAGCATC_3TCTA_2TC$-3′, reverse: 5′-$CT_2CAGT_2CGACACAG_2TCATC$-3′; *Tbp*, forward: 5′-$AGTGC_3AGCATCACTGT_3$-3′, reverse: 5′-$G_2TC_2ATGACTCTCACT_3CT_2$-3′. The PCR conditions were 95°C for 3 min, followed by 40 cycles of 95°C for 10 s and 55°C for 30 s. Relative expression levels were calculated from the average threshold cycle number using the delta-delta Ct method.

***Fluorescence Microscopy and Image Analysis.***

Cell imaging was performed with the EVOS FL Auto Imaging System (Thermo Fisher Scientific). Puncta formation and puncta indexes were analyzed as described [38]. Briefly, the redistribution of green fluorescence (N-TASQ) into punctate structures was reflected by *the puncta index*, which is the standard deviation of the intensities measured among pixels within the cellular region of interest (the nucleus, the DAPI staining). Diffuse localization corresponds to a low puncta index, and punctate localization corresponds to a high puncta index.

Photoswitching of Dendra2-LC3 was performed with the EVOS automated microscope (Thermo Fisher Scientific) as previously described [49]. Upon irradiation with blue visible light, Dendra2 undergoes an irreversible conformational change. Dendra2's spectral properties then change from that of a protein that absorbs blue light and emits green fluorescence to that of one that absorbs green light and emits red fluorescence. Photoswitched Dendra2 maintains these spectral properties until the cell degrades the protein. The red fluorescence intensities from a region of interest in individual astrocytes were measured at different time points with the EVOS

microscope. The decays of red fluorescence were plotted against time, transformed into log values, and individual half-life ($t_{1/2}$) was analyzed. $t_{1/2} = (\mathrm{Ln}(2)/\lambda)$, were $\lambda$ is the decay value.

Astrocytes were imaged with the Nikon A1R confocal laser microscope (Nikon Corporation) with the 100X Plan-Apo/1.4 NA oil lens. N-TASQ was imaged with the 488 nm laser and the DAPI dye was imaged with the 405 nm laser. Analyses were done blinded to treatment group.

***Ethics Statement.***

Rats were maintained in accordance with guidelines and regulations of the University of Texas McGovern Medical School at Houston. All experimental procedures were approved by the University of Texas McGovern Medical School at Houston.

***Statistical Analysis.***

GraphPad Prism was used to perform statistical analyses. Statistical tests are denoted within each figure legend.

**Disclosure of Potential Conflicts of Interest**

No potential conflicts of interest are disclosed.

**Acknowledgements**

We thank members of the AST and LDM laboratories for useful discussions. We apologize to all authors whose work we could not cite due to reference number constraints.

**Funding**

This work was supported by the University of Texas McGovern Medical School at Houston (A.S.T.), the RF1AG057576 grant from the National Institute on Aging (A.U.), the GM116007 grant from the National Institute of General Medical Sciences (N.K.), the AU1875 grant from the Welch Foundation (N.K.), the ANR-17-CE17-0010-01 grant from the Agence Nationale de la Recherche (D.M.), and the R01NS094543 grant from the National Institute of Neurological Disorders and Stroke (L.D.M.).

**References**

1. Rhodes D, Lipps HJ. G-quadruplexes and their regulatory roles in biology. Nucleic Acids Res 2015; 43:8627-37.
2. Maizels N, Gray LT. The G4 genome. PLoS Genet 2013; 9:e1003468.
3. Huppert JL, Balasubramanian S. Prevalence of quadruplexes in the human genome. Nucleic Acids Res 2005; 33:2908-16.
4. Eddy J, Maizels N. Gene function correlates with potential for G4 DNA formation in the human genome. Nucleic Acids Res 2006; 34:3887-96.
5. Huppert JL, Balasubramanian S. G-quadruplexes in promoters throughout the human genome. Nucleic Acids Res 2007; 35:406-13.
6. Raiber EA, Kranaster R, Lam E, Nikan M, Balasubramanian S. A non-canonical DNA structure is a binding motif for the transcription factor SP1 in vitro. Nucleic Acids Res 2012; 40:1499-508.
7. Gray LT, Vallur AC, Eddy J, Maizels N. G quadruplexes are genomewide targets of transcriptional helicases XPB and XPD. Nat Chem Biol 2014; 10:313-8.
8. Paeschke K, Bochman ML, Garcia PD, Cejka P, Friedman KL, Kowalczykowski SC, et al. Pif1 family helicases suppress genome instability at G-quadruplex motifs. Nature 2013; 497:458-62.
9. Sauer M, Paeschke K. G-quadruplex unwinding helicases and their function in vivo. Biochem Soc Trans 2017.
10. Chen MC, Tippana R, Demeshkina NA, Murat P, Balasubramanian S, Myong S, et al. Structural basis of G-quadruplex unfolding by the DEAH/RHA helicase DHX36. Nature 2018; 558:465-9.
11. Nguyen GH, Tang W, Robles AI, Beyer RP, Gray LT, Welsh JA, et al. Regulation of gene expression by the BLM helicase correlates with the presence of G-quadruplex DNA motifs. Proc Natl Acad Sci U S A 2014; 111:9905-10.
12. Tang W, Robles AI, Beyer RP, Gray LT, Nguyen GH, Oshima J, et al. The Werner syndrome RECQ helicase targets G4 DNA in human cells to modulate transcription. Hum Mol Genet 2016; 25:2060-9.
13. Lopez CR, Singh S, Hambarde S, Griffin WC, Gao J, Chib S, et al. Yeast Sub1 and human PC4 are G-quadruplex binding proteins that suppress genome instability at co-transcriptionally formed G4 DNA. Nucleic Acids Res 2017.
14. Maizels N. G4-associated human diseases. EMBO Rep 2015; 16:910-22.
15. Haeusler AR, Donnelly CJ, Rothstein JD. The expanding biology of the C9orf72 nucleotide repeat expansion in neurodegenerative disease. Nat Rev Neurosci 2016; 17:383-95.
16. Balendra R, Isaacs AM. C9orf72-mediated ALS and FTD: multiple pathways to disease. Nature Reviews Neurology 2018; 14:544-58.
17. Fry M, Loeb LA. Human werner syndrome DNA helicase unwinds tetrahelical structures of the fragile X syndrome repeat sequence d(CGG)n. J Biol Chem 1999; 274:12797-802.
18. Karikkineth AC, Scheibye-Knudsen M, Fivenson E, Croteau DL, Bohr VA. Cockayne syndrome: Clinical features, model systems and pathways. Ageing Res Rev 2016.
19. Mendoza O, Bourdoncle A, Boule JB, Brosh RM, Jr., Mergny JL. G-quadruplexes and helicases. Nucleic Acids Res 2016; 44:1989-2006.

20. Galluzzi L, Baehrecke EH, Ballabio A, Boya P, Bravo-San Pedro JM, Cecconi F, et al. Molecular definitions of autophagy and related processes. EMBO J 2017; 36:1811-36.
21. Lubas M, Harder LM, Kumsta C, Tiessen I, Hansen M, Andersen JS, et al. eIF5A is required for autophagy by mediating ATG3 translation. EMBO Rep 2018; 19.
22. Artal-Martinez de Narvajas A, Gomez TS, Zhang JS, Mann AO, Taoda Y, Gorman JA, et al. Epigenetic regulation of autophagy by the methyltransferase G9a. Mol Cell Biol 2013; 33:3983-93.
23. Baek SH, Kim KI. Epigenetic Control of Autophagy: Nuclear Events Gain More Attention. Mol Cell 2017; 65:781-5.
24. Hansen M, Rubinsztein DC, Walker DW. Autophagy as a promoter of longevity: insights from model organisms. Nature Reviews Molecular Cell Biology 2018.
25. Fernandez AF, Sebti S, Wei Y, Zou Z, Shi M, McMillan KL, et al. Disruption of the beclin 1-BCL2 autophagy regulatory complex promotes longevity in mice. Nature 2018; 558:136-40.
26. Lapierre LR, Kumsta C, Sandri M, Ballabio A, Hansen M. Transcriptional and epigenetic regulation of autophagy in aging. Autophagy 2015; 11:867-80.
27. Lipinski MM, Zheng B, Lu T, Yan Z, Py BF, Ng A, et al. Genome-wide analysis reveals mechanisms modulating autophagy in normal brain aging and in Alzheimer's disease. Proc Natl Acad Sci U S A 2010; 107:14164-9.
28. Crews L, Spencer B, Desplats P, Patrick C, Paulino A, Rockenstein E, et al. Selective molecular alterations in the autophagy pathway in patients with Lewy body disease and in models of alpha-synucleinopathy. PLoS One 2010; 5:e9313.
29. Komatsu M, Wang QJ, Holstein GR, Friedrich VL, Jr., Iwata J, Kominami E, et al. Essential role for autophagy protein Atg7 in the maintenance of axonal homeostasis and the prevention of axonal degeneration. Proc Natl Acad Sci U S A 2007; 104:14489-94.
30. Friedman LG, Lachenmayer ML, Wang J, He L, Poulose SM, Komatsu M, et al. Disrupted Autophagy Leads to Dopaminergic Axon and Dendrite Degeneration and Promotes Presynaptic Accumulation of alpha-Synuclein and LRRK2 in the Brain. J Neurosci 2012; 32:7585-93.
31. Eisenberg T, Knauer H, Schauer A, Buttner S, Ruckenstuhl C, Carmona-Gutierrez D, et al. Induction of autophagy by spermidine promotes longevity. Nat Cell Biol 2009; 11:1305-14.
32. Eisenberg T, Schroeder S, Andryushkova A, Pendl T, Kuttner V, Bhukel A, et al. Nucleocytosolic depletion of the energy metabolite acetyl-coenzyme a stimulates autophagy and prolongs lifespan. Cell Metab 2014; 19:431-44.
33. Moruno-Manchon JF, Lejault P, Wang Y, McCauley B, Honarpisheh P, Morales Scheihing DA, et al. Small-molecule G-quadruplex stabilizers reveal a novel pathway of autophagy regulation in neurons. eLife 2020; 9:e52283.
34. Rodriguez R, Miller KM, Forment JV, Bradshaw CR, Nikan M, Britton S, et al. Small-molecule-induced DNA damage identifies alternative DNA structures in human genes. Nat Chem Biol 2012; 8:301-10.
35. Neidle S. Quadruplex Nucleic Acids as Novel Therapeutic Targets. J Med Chem 2016; 59:5987-6011.
36. Cimino-Reale G, Zaffaroni N, Folini M. Emerging Role of G-quadruplex DNA as Target in Anticancer Therapy. Curr Pharm Des 2016; 22:6612-24.
37. Rosu F, De Pauw E, Gabelica V. Electrospray mass spectrometry to study drug-nucleic acids interactions. Biochimie 2008; 90:1074-87.

38. Moruno-Manchon JF, Uzor NE, Ambati CR, Shetty V, Putluri N, Jagannath C, et al. Sphingosine kinase 1-associated autophagy differs between neurons and astrocytes. Cell Death Dis 2018; 9:521.
39. Moruno-Manchon JF, Koellhoffer EC, Gopakumar J, Hambarde S, Kim N, McCullough LD, et al. The G-quadruplex DNA stabilizing drug pyridostatin promotes DNA damage and downregulates transcription of Brca1 in neurons. Aging (Albany NY) 2017; 9:1957-70.
40. Kulkarni A, Dong A, Kulkarni VV, Chen J. Differential regulation of autophagy during metabolic stress in astrocytes and neurons. 2019:1-17.
41. Lavieu G, Scarlatti F, Sala G, Carpentier S, Levade T, Ghidoni R, et al. Regulation of autophagy by sphingosine kinase 1 and its role in cell survival during nutrient starvation. The Journal of biological chemistry 2006; 281:8518-27.
42. Moruno Manchon JF, Uzor NE, Finkbeiner S, Tsvetkov AS. SPHK1/sphingosine kinase 1-mediated autophagy differs between neurons and SH-SY5Y neuroblastoma cells. Autophagy 2016; 12:1418-24.
43. Laguerre A, Hukezalie K, Winckler P, Katranji F, Chanteloup G, Pirrotta M, et al. Visualization of RNA-Quadruplexes in Live Cells. J Am Chem Soc 2015; 137:8521-5.
44. Laguerre A, Wong JM, Monchaud D. Direct visualization of both DNA and RNA quadruplexes in human cells via an uncommon spectroscopic method. Sci Rep 2016; 6:32141.
45. Stefan L, Monchaud D. Applications of guanine quartets in nanotechnology and chemical biology. Nature Reviews Chemistry 2019; 3:650-68.
46. Yang SY, Lejault P, Chevrier S, Boidot R, Robertson AG, Wong JMY, et al. Transcriptome-wide identification of transient RNA G-quadruplexes in human cells. Nature Communications 2018; 9:4730.
47. Kamura T, Katsuda Y, Kitamura Y, Ihara T. G-quadruplexes in mRNA: A key structure for biological function. Biochemical and biophysical research communications 2020.
48. Neal M, Richardson JR. Epigenetic regulation of astrocyte function in neuroinflammation and neurodegeneration. Biochimica et Biophysica Acta (BBA) - Molecular Basis of Disease 2018; 1864:432-43.
49. Tsvetkov AS, Arrasate M, Barmada S, Ando DM, Sharma P, Shaby BA, et al. Proteostasis of polyglutamine varies among neurons and predicts neurodegeneration. Nature chemical biology 2013; 9:586-92.
50. Rosu F, Gabelica V, Poncelet H, De Pauw E. Tetramolecular G-quadruplex formation pathways studied by electrospray mass spectrometry. Nucleic Acids Res 2010; 38:5217-25.

**Figure Legends**

**Figure 1.** The stoichiometry and equilibrium binding constant of the non-covalent *Atg7-32*/PDS complexes. (**A**) A scheme of the rat *Atg7* gene and its promoter showing putative G4-DNA locations. PQFSes in *Atg7* and in its promoter were analyzed by using the QGRS mapper (http://bioinformatics.ramapo.edu/QGRS/index.php). 5,000 nt upstream the start codon were analyzed. (**B-D**) Electrospray ionization mass spectrometry (ESI-MS) experiments performed with *Atg7-32* alone (10 µM) (B) or in presence of 1 and 2 mol. equiv. PDS (C, D, respectively). Mixtures were prepared in 100 mM ammonium acetate buffer and equilibrated at 25°C for 1 h

prior to the experiments (20% of methanol added to the solution for the injection, performed at a flow rate of 10 µL/min). K=4.82x10$^5$ M$^{-1}$ (C), K=1.47x10$^7$ M$^{-1}$ (D). (**E-G**) ESI-MS experiments performed with mut*Atg7-32* alone (10 µM) (E) or in presence of 1 and 2 mol. equiv. PDS (F, G, respectively). Mixtures were prepared in 100 mM ammonium acetate buffer and equilibrated at 25°C for 1 h prior to the experiments (20% of methanol added to the solution for the injection, performed at a flow rate of 10 µL/min). K=2.19x10$^4$ M$^{-1}$ (F), K=7.73x10$^4$ M$^{-1}$ (G).

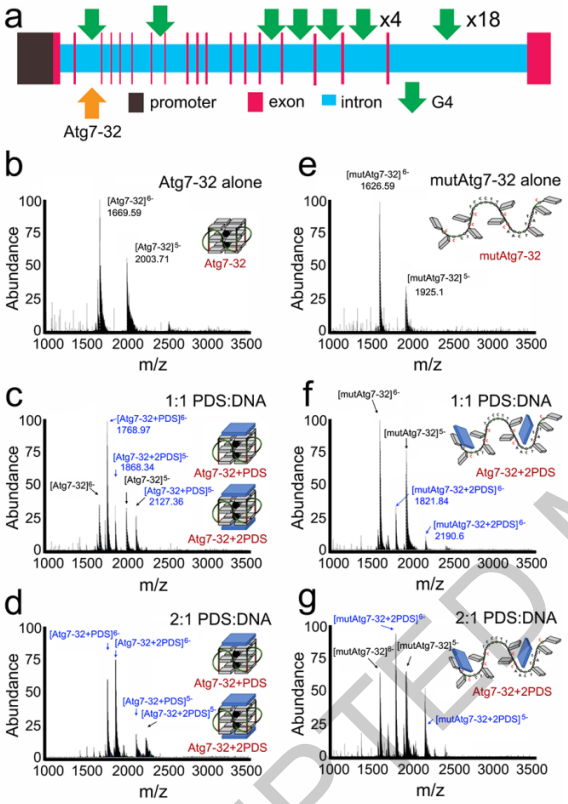


**Figure 2.** PDS downregulates the ATG7 protein and the expression of *Atg7* in astrocytes. (**A**) Primary astrocytes were cultured for 3 weeks from cortical tissue isolated from rat embryos. Cultures were fixed and stained with Alexa Fluor 633 phalloidin (red), DAPI (blue), and an antibody against GFAP (green). Most cells stained with phalloidin were positive for GFAP (94 ± 6%). Over 200 cells were analyzed, and results were pooled from three independent experiments. Scale bar: 40 µm. (**B**) Cultured primary astrocytes were treated with a vehicle (control) or with PDS (2 µM) overnight. Astrocytes were then processed to measure mRNA levels. Expression levels of *Atg7* and *Tbp* (housekeeping gene as control) were determined by qRT-PCR. *Atg7 :* p=0.017 (t-test), *p<0.05 ; *Tbp* : p=0.7949 (t-test), n.s., non-significant. Results were pooled from six experiments. (**C**) Cultured primary astrocytes were treated with a vehicle (control) or

with PDS (2 µM) overnight. Astrocytes were then processed to measure the levels of ATG7 and SQSTM1. ATG7: *p=0.019 (t-test), SQSTM1: *p=0.018 (t-test). Results were pooled from six experiments. (**D**) An example of western blotting experiments in (C). (**E**) Dendra2-LC3 was used to measure autophagy flux. Two cohorts of astrocytes were co-transfected with Dendra2-LC3 and an empty plasmid, or with Dendra2-LC3 and untagged SPHK1 (sphingosine kinase 1, a positive control). Astrocytes co-transfected with Dendra2-LC3 and an empty plasmid were treated with a vehicle (control, cont), or with 0.5 µM PDS overnight. After treatment, cells were photoswitched and longitudinally imaged, and the decay of the red fluorescence over time was used to calculate the half-life of Dendra2-LC3. The half-life of Dendra2-LC3 is normalized to one with respect to control astrocytes. cont vs SK1: *p=0.001, cont vs PDS : **p=0.001, SK1 vs PDS : **p=0.001 (one-way ANOVA followed by Tukey's multiple comparisons testing). Fifty cells per group were analyzed from two independent experiments. (**F**) An example of a photoswitching experiment with Dendra2-LC3 and SPHK1 (untagged). Astrocytes co-transfected with Dendra2-LC3 and SPHK1 were treated with a vehicle overnight. Cells were photoswitched and longitudinally imaged. Autophagosomes are depicted with white arrows. Blue arrow depicts photoswitching. Scale bar: 25 µm.

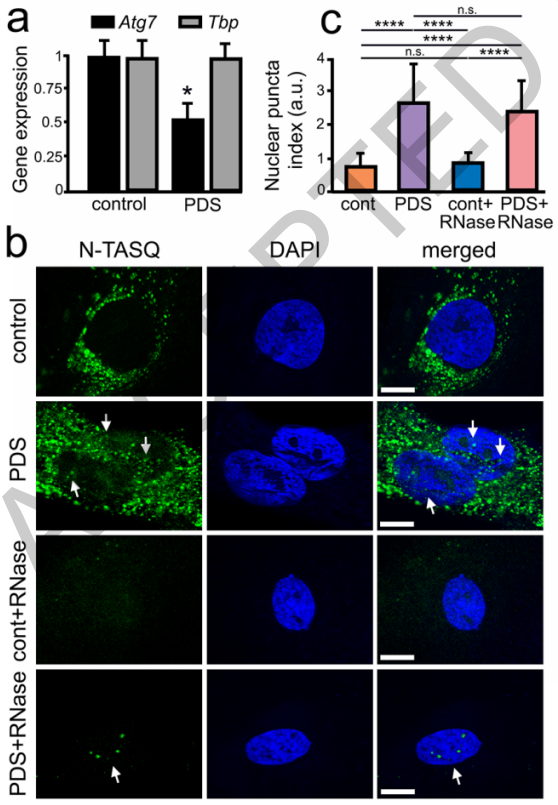

**Figure 3.** PDS alters G4 landscapes in astrocytes. (**A**) Cultured primary astrocytes were treated with a vehicle (control) or with PDS (2 μM) overnight. Cells were fixed and stained with N-TASQ (50 μM) and with the nuclear dye Hoechst (DAPI). Some samples were treated with RNase to digest RNA before staining. Fixed cells were automatically imaged with the EVOS microscope (N-TASQ and DAPI) and the nuclear puncta index was analyzed in all conditions. Two-way ANOVA followed by Tukey's multiple comparisons test were used. ****$p<0.0001$, n.s., non-significant. For each experiment, 80 cells were blindly analyzed, and results were pooled from two independent experiments. (**B**) The number of puncta was analyzed in cells from (A) with ImageJ. Two-way ANOVA followed by Tukey's multiple comparisons test were used. ****$p<0.0001$, n.s., non-significant. (**C**) Cultured primary astrocytes were treated with a vehicle (control) or with PDS (2 μM) overnight. Cells were fixed and stained with N-TASQ (50 μM) and with the nuclear dye Hoechst (DAPI). Some samples were treated with RNase to digest RNA before staining. Fixed cells were analyzed with a confocal microscope (N-TASQ and DAPI). Scale bar: 1 μm.